

# Bioinspired model of mechanical energy harvesting based on flexoelectric membranes

Alejandro D. Rey,\* P. Servio, and E. E. Herrera-Valencia

*Department of Chemical Engineering, McGill University, Montreal, Quebec, Canada H3A 2B2*

(Received 16 September 2012; published 19 February 2013)

Membrane flexoelectricity is an electromechanical coupling process that describes membrane electrical polarization due to bending and membrane bending under electric fields. In this paper we propose, formulate, and characterize a mechanical energy harvesting system consisting of a deformable soft flexoelectric thin membrane subjected to harmonic forcing from contacting bulk fluids. The key elements of the energy harvester are formulated and characterized, including (i) the mechanical-to-electrical energy conversion efficiency, (ii) the electromechanical shape equation connecting fluid forces with membrane curvature and electric displacement, and (iii) the electric power generation and efficiency. The energy conversion efficiency is cast as the ratio of flexoelectric coupling to the product of electric and bending elasticity. The device is described by a second-order curvature dynamics coupled to the electric displacement equation and as such results in mechanical power absorption with a resonant peak whose amplitude decreases with bending viscosity. The electric power generation is proportional to the conversion factor and the power efficiency decreases with frequency. Under high bending viscosity, the power efficiency increases with the conversion factor and under low viscosities it decreases with the conversion factor. The theoretical results presented contribute to the ongoing experimental efforts to develop mechanical energy harvesting from fluid flow energy through solid-fluid interactions and electromechanical transduction.

DOI: [10.1103/PhysRevE.87.022505](https://doi.org/10.1103/PhysRevE.87.022505)

PACS number(s): 83.80.Xz, 61.30.Cz, 61.30.Eb, 46.70.Hg

## I. INTRODUCTION

Energy harvesting based on mechanical oscillations using active materials is a quickly evolving and promising interdisciplinary area of electric energy production [1–9]. The sources of mechanical oscillations include solid mechanical vibrations, fluid flow instabilities, and traveling and standing wave motion. The active materials in energy harvesting must display sensor and actuator capabilities arising from specific molecular composition and architectures [2]. Commonly, sensor abilities rely on materials that respond electrically to mechanical excitation. On the other hand actuation relies on converting a nonmechanical electric stimulus into a displacement or shape change. Energy harvesting using ambient mechanical vibrations is based on materials with adequate electromechanical couplings, with piezoelectricity being the most actively pursued, based on ceramics [piezoelectric lead zirconium titanate (PZT)], polymers [polyvinylidene difluoride (PVDF)], and piezocomposites (macrofiber composites) [2,5–9]. Other polymeric materials for mechanical energy harvesting include electrostrictive, dielectric, electroactive, conductive, and ionic polymer metal composites, and are being investigated as alternatives to electromagnetism, electrostatics, or piezoelectricity, which perform at large frequencies [2]. In this paper we analyze and model another alternative based on membrane flexoelectricity that combines the polarization abilities of liquid crystals with the soft bending elasticity associated with thin membranes [10–15]. The motivation of this work stems from the development of new materials with encouraging flexoelectric properties [16,17].

Next we very briefly describe the piezoelectric approach to fluid-based mechanical energy harvesting which serves as a significant guideline for the less established membrane flexoelectric electromechanical transduction method presented

in this paper [8,9]. Piezoelectrical materials generate electric displacement when a mechanical stress is applied; this is known as the sensor mode or direct effect:  $P_{i\text{piezo}} = d_{ijk}T_{jk}$ . The  $\mathbf{d}$  tensor is the piezoelectric charge tensor and sets the charge separation produced by an applied stress. Piezoelectrics also display an electrical-to-mechanical actuation effect, such that a strain deformation  $S_{ij}$  is generated when an electric field  $\mathbf{E}$  is applied,  $S_{ij} = d_{ijk}E_k$ . In energy harvesting applications both the direct and inverse effects are involved; the direct effect is used for charge generation (the sensor) and this is followed by feedback through the inverse effect that provides actuation (the motor) through strain. The integrated motor-generator model that couples strain  $\mathbf{S}$ , displacement  $\mathbf{D}$ , stress  $\mathbf{T}$ , and electrical field  $\mathbf{E}$  is given in the following different formats as

$$\begin{aligned}
 \begin{pmatrix} \text{actuator/motor} \\ \text{sensor/generator} \end{pmatrix} &\Rightarrow \begin{pmatrix} \mathbf{T} \\ \mathbf{E} \end{pmatrix} = \underbrace{\begin{pmatrix} \mathbf{c}^D & -\mathbf{q}^\dagger \\ -\mathbf{q} & (\boldsymbol{\epsilon}^S)^{-1} \end{pmatrix}}_{\text{stress-voltage}} \otimes \begin{pmatrix} \mathbf{S} \\ \mathbf{D} \end{pmatrix}, \\
 \begin{pmatrix} \mathbf{S} \\ \mathbf{E} \end{pmatrix} &= \underbrace{\begin{pmatrix} \mathbf{s}^D & \mathbf{g}^\dagger \\ -\mathbf{g} & (\boldsymbol{\epsilon}^T)^{-1} \end{pmatrix}}_{\text{strain-voltage}} \otimes \begin{pmatrix} \mathbf{T} \\ \mathbf{D} \end{pmatrix}, \\
 \begin{pmatrix} \text{actuator/motor} \\ \text{sensor/generator} \end{pmatrix} &\Rightarrow \begin{pmatrix} \mathbf{T} \\ \mathbf{D} \end{pmatrix} = \underbrace{\begin{pmatrix} \mathbf{c}^E & -\mathbf{e}^\dagger \\ \mathbf{e} & \boldsymbol{\epsilon}^S \end{pmatrix}}_{\text{stress-charge}} \otimes \begin{pmatrix} \mathbf{S} \\ \mathbf{E} \end{pmatrix}, \\
 \begin{pmatrix} \mathbf{S} \\ \mathbf{D} \end{pmatrix} &= \underbrace{\begin{pmatrix} \mathbf{s}^E & \mathbf{d}^\dagger \\ \mathbf{d} & \boldsymbol{\epsilon}^\dagger \end{pmatrix}}_{\text{strain-charge}} \otimes \begin{pmatrix} \mathbf{T} \\ \mathbf{E} \end{pmatrix},
 \end{aligned} \tag{1}$$

where  $\mathbf{c}$  is the stiffness tensor,  $\mathbf{s} = (\mathbf{c})^{-1}$  is the compliance,  $\boldsymbol{\epsilon}$  is the permittivity tensor,  $(\boldsymbol{\epsilon})^{-1}$  is the inverse electric permittivity,

\*alejandro.rey@mcgill.ca

$\mathbf{e}$ ,  $\mathbf{d}$ ,  $\mathbf{q}$ , and  $\mathbf{g}$  are the piezoelectric coupling coefficients; a superscript denotes that the designated field is set equal to zero (e.g.,  $\mathbf{s}^D$  and  $\boldsymbol{\epsilon}^S$  mean compliance at zero displacement and permittivity tensor at zero stiffness, respectively), a superscript  $\dagger$  denotes the transpose, and  $\otimes$  denotes the proper tensor product. Relations such as  $\mathbf{c}^D = \mathbf{c}^E + \mathbf{e}^\dagger \cdot (\boldsymbol{\epsilon}^S)^{-1} \cdot \mathbf{e}$  and

$\mathbf{s}^D = \mathbf{s}^E - \mathbf{d}^\dagger \cdot (\boldsymbol{\epsilon}^\dagger)^{-1} \cdot \mathbf{d}$  between the property tensors at different conditions follow directly from cross substitutions in Eqs. (1). The piezoelectric conversion coefficient  $k_{ij}^2$ ,  $i, j = 33, 31$ , is an index of merit that quantifies the fraction of the energy converted between the mechanical and electrical domains and is bounded as [8,9]

$$0 < k_{ij}^2 = \frac{\text{transformed energy}}{\text{incoming energy}} = \frac{(\text{interaction})^2}{\text{elastic} \times \text{dielectric}} = \frac{d_{ij}}{\sqrt{\epsilon_{ij}^\dagger s_{ij}^E}} < 1, \quad (2)$$

were we used the strain-charge (actuator) configuration; the other expressions can be read from Eqs. (1). The higher the  $k_{ij}^2$  the higher the electromechanical energy conversion. Integrating the generator-motor equations with the Navier-Stokes equations for fluid flow gives a generic model for energy harvesting from fluid-flow-generated mechanical oscillations [4]:

$$\left. \begin{array}{l} \text{fluid flow} \\ \left\{ \begin{array}{l} \frac{d\rho}{dt} + \rho \nabla \cdot \mathbf{v} = 0 \\ \rho \frac{d\mathbf{v}}{dt} = -\nabla p + \nabla \cdot \mathbf{T}_f \end{array} \right\} \end{array} \right\} \xleftrightarrow{\mathbf{f}_f} \left. \begin{array}{l} \text{solid elasticity} \\ \left\{ \rho \frac{d^2 \mathbf{u}}{dt^2} = \nabla \cdot \mathbf{T} + \mathbf{f}_f \right\} \end{array} \right\} \xleftrightarrow{\begin{pmatrix} \mathbf{T} \\ \mathbf{E} \end{pmatrix} = \begin{pmatrix} \mathbf{c}^D & -\mathbf{q}^\dagger \\ -\mathbf{q} & (\boldsymbol{\epsilon}^S)^{-1} \end{pmatrix} \begin{pmatrix} \mathbf{S} \\ \mathbf{D} \end{pmatrix}} \left. \begin{array}{l} \text{Gauss law} \\ \{\nabla \cdot \mathbf{D} = q_f\} \end{array} \right\} \quad (3)$$

The text in the top row defines the mechanism; the corresponding equations are given in braces below and the symbols below the double arrows indicate the connecting terms between two processes. This system of equations (3) shows the integrated coupling between a fluid's linear momentum, the piezoelectric solid elasticity, and the Gauss law. Fluid flow stresses  $\mathbf{T}_f$  from unsteady fluid flows act on the solid elastic material, generating strains  $\mathbf{S}$  ( $2\mathbf{S} = \nabla \mathbf{u} + \nabla \mathbf{u}^\dagger$ , where  $\mathbf{u}$  is the displacement) that couple through piezoelectricity with the generator equation ( $\mathbf{D}$ ), resulting in the conversion of fluid flow into mechanical and electrical energy;  $\mathbf{f}_f$  is the net force of the fluid into the solid, and  $q_f$  is the free charge density. Both air and water flows under laminar and turbulent conditions are being investigated as mechanical energy sources. The system of equations (3) will be used as a guideline to build the corresponding flexoelectric energy harvester. The overall electromechanical efficiency of the process,  $\eta$ , is the product of the efficiency of conversion of flow power to the mechanical power  $\eta_{\text{fm}}$  times the efficiency of conversion of mechanical power to electric power  $\eta_{\text{me}}$  [4]:

$$\eta = \eta_{\text{fm}} \eta_{\text{me}} = \frac{P_{\text{mech}}}{P_{\text{flow}}} \frac{P_{\text{elec}}}{P_{\text{mech}}}. \quad (4)$$

As mentioned above the basic components Eqs. (1)–(3) and the performance Eq. (4) of the piezoelectric-based mechanical energy harvester model will be used in this paper as a framework to develop a model of the flexoelectric-based harvester. The implementation of the modeling procedure, based on a correspondence with the processes given in the system of equations (3), requires a brief discussion of (i) liquid crystal and membrane flexoelectricity, (ii) sensor and actuator flexoelectric modes, and (iii) flexoelectric energy harvesting, as follows.

### A. Liquid crystal and membrane flexoelectricity

Membrane flexoelectricity [10–15] is the ability of synthetic and biological flat membranes to bend under the imposition of an external electric field (actuator), and the capacity to become polarized under bending (sensor) [10–15], which play a fundamental actuation-sensor role in the functionality of the outer hair cells of the inner ear. Figure 1 shows a flexoelectric lipid bilayer in which due to intrinsic polarization of the lipids, bending creates polarization  $\mathbf{P}$  along the membrane unit normal  $\mathbf{k}$  since the lower half surface is in compression and the top in tension.

The basic science and applications of membrane flexoelectricity were developed by Petrov and co-workers and are described in detail in Ref. [10];

### B. Sensor and actuator flexoelectric modes

The flexoelectric actuator mode is given by a linear relation between input [electric displacement  $\mathbf{D}$  (C/m)] and output [flexoelectric bending moment tensor  $\mathbf{M}^f$  (J/m)]:

$$\mathbf{M}^f = -\mathbf{D} \cdot \mathbf{h}. \quad (5)$$

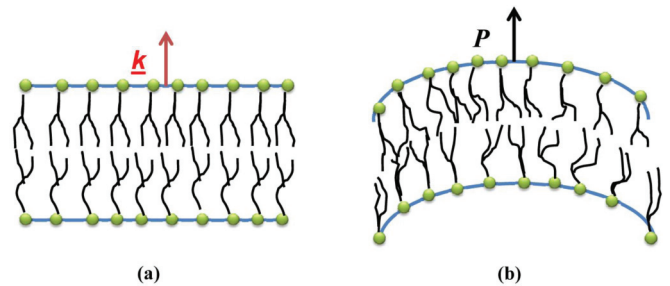


FIG. 1. (Color online) Schematic of membrane flexoelectricity in biological membranes. (a) Under planar conditions there is no polarization. (b) Under bending the lower surface is in compression and the upper one in dilation, and electric polarization is generated.

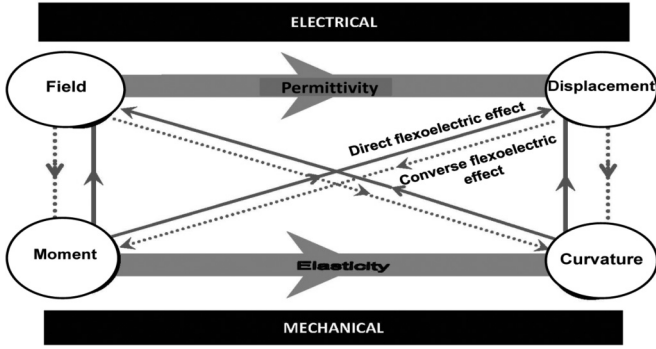


FIG. 2. Thermodynamic diagram showing the relations between electrical ( $\mathbf{E}, \mathbf{D}$ ) and mechanical ( $\mathbf{M}, \mathbf{b}$ ) quantities. The full thin lines denote the direct flexoelectric effect and the dashed lines the converse. The curvature elasticity was given by the Helfrich mechanism. Biological membrane flexoelectricity was established by Petrov [10].

The third-order membrane flexoelectric tensor is defined by the geometry of the membrane:

$$\mathbf{h} = \mathbf{k}\mathbf{k} \cdot \mathbf{h} = \mathbf{h} \cdot \mathbf{I}_s = h\mathbf{k}\mathbf{I}_s \quad (6)$$

where  $h$  is the flexoelectric constant [10–15],  $\mathbf{k}$  is the unit normal to the membrane, and  $\mathbf{I}_s = \mathbf{I} - \mathbf{k}\mathbf{k}$  is the surface unit tensor. The symmetric elastic moment tensor  $\mathbf{M}^f = -h\mathbf{D}\mathbf{I}_s$  scales with  $\mathbf{D} \cdot \mathbf{k} = D$  and vanishes under open circuit conditions. The flexoelectric sensor mode of synthetic and biological membranes is given by a linear relation between input [average curvature  $\mathbb{H}$  (1/m); see Appendix A] and output [electric field  $\mathbf{E}$  (V/m)]:

$$\mathbf{E} = -\mathbf{h} : \mathbf{b} = h\mathbf{k}(\mathbf{I}_s : \mathbf{b}) = h\mathbf{k}(2\mathbb{H}), \quad (7)$$

where  $\mathbf{b} = -\nabla_s \mathbf{k}$  is the symmetric curvature tensor [18–20],  $\mathbf{k}$  is the membrane unit normal,  $\nabla_s(\cdot) = \mathbf{I}_s \cdot \nabla(\cdot)$  is the surface gradient operator [18–20], and  $\mathbb{H} = \mathbf{I}_s : \mathbf{b}/2$  is the average curvature; see Appendix A for membrane geometry fundamentals. Membrane bending distortions hence create an electric polarization. We find the following correspondence [stress-voltage formulation in Eqs. (1)] between three-dimensional (3D) piezoelectric and 2D membrane mechanical quantities:  $\mathbf{S} \rightarrow \mathbf{b}$ ,  $\mathbf{T} \rightarrow \mathbf{M}$  and expect the following direct  $\mathbf{E}(\mathbf{D}, \mathbf{b})$  and converse  $\mathbf{M}^{fe}(\mathbf{D}, \mathbf{b})$  flexoelectric equations:

$$\mathbf{M}^{fe} = -\mathbf{D} \cdot \mathbf{h} + \mathbf{c}^D : \mathbf{b}, \quad (8a)$$

$$\mathbf{E} = \boldsymbol{\beta}^b \cdot \mathbf{D} - \mathbf{h} : \mathbf{b}, \quad (8b)$$

where  $\mathbf{M}^{fe}$  is the flexoelastic moment tensor,  $\mathbf{c}^D$  is the membrane stiffness at  $\mathbf{D} = \mathbf{0}$  and  $\boldsymbol{\beta}^b = \beta^b \mathbf{k}\mathbf{k}$  is the inverse permittivity at  $\mathbf{b} = \mathbf{0}$ . Typical characteristic values of  $|\mathbf{h}/\boldsymbol{\beta}^b|$  for dipolar lipid membranes are  $10^{-20}$  C [10]. A unique feature of membrane flexoelectricity that may prove advantageous in future applications of mechanical energy harvesting based on fluid flow is that polarization-induced bending in thin soft membranes is a natural response mode when immersing thin elastic membrane in a flow field that can be tuned to resonant conditions. Figure 2 provides an electrical-mechanical coupling diagram based on the  $\mathbf{S} \rightarrow \mathbf{b}$ ,  $\mathbf{T} \rightarrow \mathbf{M}$  correspondence. The thin lines denote the direct flexoelectric effect and the

dashed lines the converse one. The equivalent four sets of Eqs. (1) are (i) moment-voltage, (ii) curvature-voltage, (iii) moment-charge, and (iv) curvature-charge. In this work devoted to voltage generation we use the moment-charge set as shown in Eq. (8).

### C. Flexoelectric energy harvesting

This brief section presents the key material properties and geometric features of the proposed device, its foundations in the flexoelectric shape equation previously derived [18, 19], and the distinguishing features of the device-governing equation, which is derived in detail in Sec. II. To harvest mechanical energy using flexoelectric membranes, we subject the deformable flexoelectric membrane to interfacial forces from a contacting bulk fluid. The basic energy conversion steps in the proposed device are shown in Fig. 3.

The transfer of the bulk fluid mechanical energy onto the deformable flexoelectric membrane is described by the membrane shape equation or stress balance along the membrane unit normal  $\mathbf{k}$ . From previous work [18, 19] we find that the linear integral shape that describes the shape of constant curvature membranes (flat membranes that deform into spheres or cylinders) when subjected to tension, moments, and bulk fluid effects is

$$-\rho \frac{\partial V}{\partial t} + \underbrace{\mathbf{T} : \mathbf{b}}_{\text{tension}} + \underbrace{(\boldsymbol{\eta} \cdot \mathbf{M} \cdot \boldsymbol{\eta}) \mathbb{S}}_{\text{moments}} = \underbrace{\mathbf{k}\mathbf{k} : (\mathbf{T}_{b(1)} - \mathbf{T}_{b(2)})}_{\text{bulk fluids}}, \quad (9a)$$

$$\mathbf{T} : \mathbf{b}|_{\text{linearized}} = 2\gamma_{00}\mathbb{H}, \quad (9b)$$

where  $V$  is the membrane normal velocity,  $\mathbf{T} : \mathbf{b} = 2\gamma_{00}\mathbb{H}$  is the linearized membrane Laplace pressure,  $\mathbf{T}$  is the membrane stress tensor,  $\gamma_{00}$  is the tension,  $\mathbb{H}$  is the average curvature,  $\mathbf{M} = \mathbf{M}^{fe} + \mathbf{M}^v$  is the total moment tensor,  $\mathbf{M}^v$  is the viscous moment,  $\mathbf{k}\mathbf{k} : (\mathbf{T}_{b(2)} - \mathbf{T}_{b(1)})$  is the bulk stress jump between bulk fluid phases 1 and 2,  $\mathbb{S}$  is the shape area factor (units 1/area), and  $\boldsymbol{\eta}$  is a unit vector tangent to the membrane and normal to its edge. The shape area factor for a circular membrane whose edge is fixed in a capillary of radius  $a$  is  $\mathbb{S}_{\text{sphere}} = 8/a^2$ , and for a rectangular membrane attached to two vertical plates of separation distance  $2a$ ,  $\mathbb{S}_{\text{cylinder}} = 3/a^2$ . Figure 4(a) shows the capillary geometry for mechanical energy harvesting based on membrane flexoelectricity, where the membrane is attached to the wall of the capillary and coated with thin electrodes. The tube is filled with a fluid, and the oscillating pressure jump  $\mathbf{k}\mathbf{k} : (\mathbf{T}_{b(2)} - \mathbf{T}_{b(1)}) = \Delta p(t)$  across

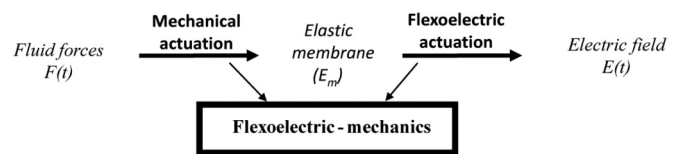


FIG. 3. Schematic of the processes and mechanisms underlying the proposed energy harvester. The fluid force  $F(t)$  distorts the membrane through momentum transfer. The membrane elastic  $E_m$  distortions are transferred to contacting electrodes and deliver electric power  $\Pi_{\text{elec}}$ . The combination of the flexoelectric sensor and mechanical actuation is called flexoelectric mechanics.

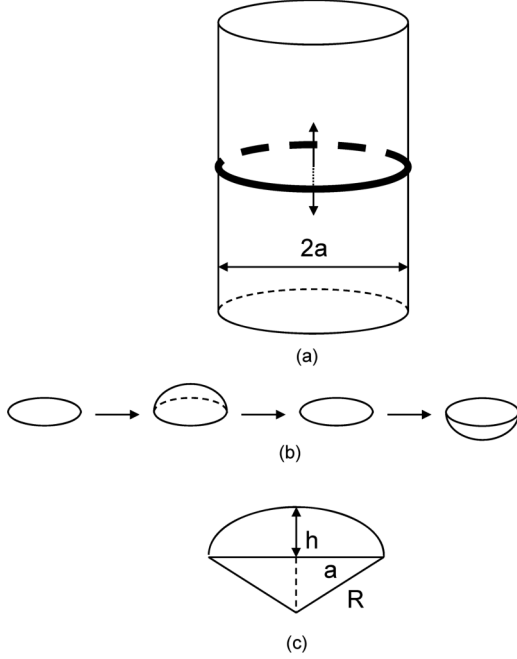


FIG. 4. (a) Schematic of a circular flexoelectric membrane coated with electrodes fixed on a capillary tube of radius  $2a$  driven by the bulk fluid pressure jump  $\Delta p(t)$  across the membrane. (b) The pressure jump oscillations create oscillations in the curvature  $\mathbb{H}$  which produce electric induction  $D(t)$ . (c) Geometry of the spherical membrane:  $h$  is the height of the spherical cap and  $R$  is the radius and the shape factor is  $\mathbb{S}_{\text{sphere}} = 8/a^2$ .

the membrane creates a periodic bending and concomitant electric response in the membrane; see Fig. 4(b).

The membrane periodically deforms into a spherical cusp of height  $h(t)$ , and radius  $R(t)$ , shown in Fig. 4(c). In the spherical cusp geometry, and with a capillary of radius  $a$ , the volume of this spherical cusp is  $\pi a^2 h(t)/2$  and the average curvature is  $\mathbb{H}(t) = -2h(t)/a^2$ ; this curvature generates the electrical polarization. Since the flexoelectric membrane subjected to contacting fluid stress is a driven viscoelastic-inertial system, the curvature dynamics  $\mathbb{H}$  found from Eqs. (9) is a second-order oscillator [21]:

$$\frac{d^2 \mathbb{H}}{dt^2} + \bar{\lambda} \frac{d\mathbb{H}}{dt} + \omega_0^2 \mathbb{H} = f(t, \mathbf{D}). \quad (10)$$

Adjusting the natural frequency  $\omega_0$  to the input  $f(t, \mathbf{D})$  through the membrane bending resistance and minimizing the membrane bending viscosity  $\bar{\lambda}$  can lead to enhanced energy harvesting.

The objective of this paper is to develop a model of a membrane flexoelectric mechanical energy harvesting system based on the following sequence of steps: (i) We develop the equivalent to the fluid-solid-piezoelectric coupled system Eqs. (8); the solid in Eq. (3) now becomes a deformable membrane with bending resistance and the piezoelectric electromechanical transduction mechanism is now flexoelectricity. (ii) The solid force balance equation used in piezoelectricity now is the membrane shape equation which has to be formulated and coupled to the fluid and to the Gauss law. (iii) Then we formulate the efficiency of the energy

harvesting process, equivalent to the piezoelectric harvester Eqs. (8). The significance of the formulated device model based on soft matter membranes is that it clearly identifies the specific geometric parameters, membrane viscoelastic moduli, and forcing frequency that control the power efficiency. In particular, the model can quantify how the membrane bending viscosity and bending modulus affect voltage generation and what frequency regimes are expected in the harvester. The theoretical predictions presented here are inspired by biological flexoelectric membranes, whose role in mechanical power generation has been formulated previously to simulate the functioning of the outer hair cells of the inner ear [21]. More quantitative predictions can be made in the future, as more experimental and molecular simulation data becomes available on flexoelectric membranes.

The organization of this paper is as follows. Section II develops the equations of flexoelasticity, starting with the Helmholtz flexoelectric membrane free energy density  $\bar{A}(\rho, \mathbf{b}, \mathbf{D})$ ; Appendix A presents all the required differential geometry used in this paper and Appendix B presents the details of the derivation of the Helmholtz free energy density  $\bar{A}(\rho, \mathbf{b}, \mathbf{D})$ . This energy is then used to derive the membrane tension  $\gamma$  for curved polarized membranes, the flexoelastic moment tensor  $\mathbf{M}^{\text{fe}}$ , the stress tensor  $\mathbf{T}$ , and the flexoelectric coupling constant  $k^2$ . Section III develops the viscoelastic-inertial dynamics of a circular membrane fixed in a capillary tube and coated with electrodes and subjected to a harmonic pressure jump  $\Delta p(\omega, t)$ . Short and open circuit analysis of mechanical power, resonance, and short circuit current and open circuit voltage are presented. The electric power is derived in terms of the product of the latter quantities and a fill factor. In the last section IV, we summarize the findings and discuss their significance in terms of the effect of fluid forces, flexoelectric material properties, and imposed frequency on power generation, and finally develop an index of merit for the efficiency.

## II. FLEXOELASTICITY

In this section we first derive the Helmholtz membrane free energy density  $\bar{A}$  and then use it to formulate the membrane tension  $\gamma$ , flexoelastic moment tensor  $\mathbf{M}^{\text{fe}}$ , and stress tensor  $\mathbf{T}$  needed to obtain the flexoelectric coupling constant  $k^2$ .

### A. Helmholtz flexoelectric membrane free energy density $\bar{A}(\rho, \mathbf{b}, \mathbf{D})$

Here we derive the free energy density per unit area  $\bar{A}(\rho, \mathbf{b}, \mathbf{D})$  as a function of the surface density  $\rho$ , the  $2 \times 2$  symmetric curvature tensor  $\mathbf{b} = \mathbb{H}\mathbf{I}_s + \mathbb{D}\mathbf{q}^*$ , and the surface displacement  $\mathbf{D}$  (charge/length);  $\mathbb{D}$  is the deviatoric curvature and  $\mathbb{K} = \mathbb{H}^2 - \mathbb{D}^2$  is the Gaussian curvature. The change of total internal energy  $U$  due to entropy  $S_{\text{ent}}$  change, deformation  $\delta W_{\text{def}}$ , shape  $\delta W_{\text{shape}}$ , and electrical  $\delta W_{\text{elec}}$  work is

$$dU = \Theta dS_{\text{ent}} + \delta W_{\text{def}} + \delta W_{\text{shape}} + \delta W_{\text{elec}}, \quad (11)$$

where  $\Theta$  is the temperature and where the tension  $\gamma$ , flexoelastic moment  $\mathbf{M}^{\text{fe}}$ , and electric-field- ( $\mathbf{E}$ -) driven work on a membrane of area  $\mathbb{A}$  are

$$\delta W_{\text{def}} = \gamma d\mathbb{A}, \quad \delta W_{\text{shape}} = \mathbb{A} \mathbf{M}^{\text{fe}} : d\mathbf{b}, \quad \delta W_{\text{elec}} = \mathbf{E} \cdot d(\mathbb{A} \mathbf{D}). \quad (12)$$

Introducing areal quantities ( $\bar{U} = U/\mathbb{A}$ ) and the Helmholtz free energy density  $\bar{A} = \bar{U} - T\bar{S}_{\text{ent}}$  into Eq. (11) we find in the absence of thermal effects (see Appendix B)

$$d\bar{A} = (-\gamma + \bar{A} - \mathbf{E} \cdot \mathbf{D}) \frac{d\rho}{\rho} + \mathbf{M}^{\text{fe}} : d\mathbf{b} + \mathbf{E} \cdot d\mathbf{D}. \quad (13)$$

Introducing Eq. (8b) into Eq. (13) and integrating we find

$$\bar{A}(\rho, \mathbf{b}, \mathbf{D}) = \bar{A}_0(\rho, \mathbf{b}) - \mathbf{h} : \mathbf{b} \cdot \mathbf{D} + \frac{1}{2} \boldsymbol{\beta}^b \cdot \mathbf{D} \cdot \mathbf{D}, \quad (14)$$

where  $\bar{A}_0(\rho, \mathbf{b})$  is the purely elastic membrane component, given by the Helfrich free energy density:

$$\bar{A}_0(\rho, \mathbf{b}) = \bar{A}_{00}(\rho) + (2k_c^D + \bar{k}_c^D) \mathbb{H}^2 - \bar{k}_c^D \mathbb{D}^2, \quad (15)$$

and where  $\bar{A}_{00}(\rho)$  is the density,  $(2k_c^D + \bar{k}_c^D) \mathbb{H}^2$  the bending, and  $-\bar{k}_c^D \mathbb{D}^2$  the torsion contributions.  $k_c$  and  $\bar{k}_c$  are the bending and torsion (also known as Gaussian rigidity or saddle-splay) elastic moduli (see, for example, Kralchevski and Nagayama [20]). Experimental values for  $k_c$  have long been reported for many biological and synthetic membranes but direct measurement methods are complicated and very recent [22,23]. Direct measurement methods of the saddle-splay modulus  $\bar{k}_c$  are not available, since with a constant Euler characteristic this term does not contribute to the bulk equations; on the other hand Eq. (15) of Ljunggren *et al.* [24] shows the role  $\bar{k}_c$  plays in the boundary conditions of freely hinged membranes. Using  $\mathbf{h} = h_f \mathbf{k} \mathbf{I}_s$ ,  $\boldsymbol{\beta}^b = \beta \mathbf{k} \mathbf{k}$  and  $D = \mathbf{D} \cdot \mathbf{k}$ , dictated from the symmetry of the thin membrane, the Helmholtz free energy density becomes

$$\begin{aligned} \bar{A}(\rho, \mathbf{b}, D) = & \bar{A}_{00}(\rho) + (2k_c^D + \bar{k}_c^D) \mathbb{H}^2 - \bar{k}_c^D \mathbb{D}^2 \\ & - 2h_f \mathbb{H} D + \frac{1}{2} \beta^b D^2. \end{aligned} \quad (16)$$

The free energy  $\bar{A}(\rho, \mathbf{b}, D)$  has mechanical, coupling, and electrical contributions. The flexoelastic coupling term  $-2h_f \mathbb{H} D$  involves only the average curvature. For spheres  $\mathbb{D} = 0$  and for cylinders  $\mathbb{H} = \mathbb{D}$ .

## B. Tension, flexoelastic moment tensor, and electric field

Equation (13) gives the following tension  $\gamma$ , flexoelastic moment tensor  $\mathbf{M}^{\text{fe}}$ , and electric field  $\mathbf{E}$  expressions:

$$-\gamma + \bar{A} - \mathbf{E} \cdot \mathbf{D} = \rho \frac{\partial \bar{A}}{\partial \rho}, \quad (17a)$$

$$\mathbf{M}^{\text{fe}} = \frac{\partial \bar{A}}{\partial \mathbf{b}}, \quad (17b)$$

$$\mathbf{E} = \frac{\partial \bar{A}}{\partial \mathbf{D}}, \quad (17c)$$

whose detailed expressions are as follows.

### 1. Membrane tension

Equation (17a) is the surface Euler equation for polarizable membranes, which relates the free energy to the tension:  $\bar{A} = \gamma + \rho \partial \bar{A} / \partial \rho + \mathbf{E} \cdot \mathbf{D}$ . Assuming that all density effects are in  $\bar{A}_{00}(\rho)$  and using Eqs. (16) and (17a) gives the membrane tension  $\gamma$ :

$$\gamma = \gamma_{00} + (2k_c^D + \bar{k}_c^D) \mathbb{H}^2 - \bar{k}_c^D \mathbb{D}^2 - \frac{1}{2} \beta^b D D, \quad (18)$$

where  $\gamma_{00}$  is the tension at zero curvature  $\mathbb{H} = \mathbb{D} = 0$  and zero displacement  $D = 0$ . The tension  $\gamma$  is a quadratically

decreasing function of the displacement  $D$  and the bending and torsion contributions are given by the Helfrich expression [see Eq. (15)].

### 2. Flexoelastic membrane moment tensor

Equation (13) gives the flexoelastic moment tensor as the change in energy with changes in curvature:  $\mathbf{M}^{\text{fe}} = \partial \bar{A} / \partial \mathbf{b}$ . Using Eqs. (16) and (17b) we find three contributions:

$$\mathbf{M}^{\text{fe}} = \left( \frac{\mathcal{B}}{2} - h_f D \right) \mathbf{I}_s + \frac{\mathcal{T}}{2} \mathbf{q}^*, \quad (19a)$$

$$\mathcal{B} = 2(2k_c^D + \bar{k}_c^D) \mathbb{H}, \quad (19b)$$

$$\mathcal{T} = -2\bar{k}_c^D \mathbb{D}, \quad (19c)$$

where  $\mathcal{B}$  and  $\mathcal{T}$  are the bending and torsion functions. This form for  $\mathbf{M}^{\text{fe}} = \partial \bar{A} / \partial \mathbf{b}$  is consistent with a diagonalized symmetric surface tensor; see the last line on Appendix A. Flexoelectricity affects only the bending moments since polarization is generated by  $\mathbb{H}$  and not by  $\mathbb{D}$ . Using the definition  $\mathbf{M}^{\text{fe}} = -\mathbf{D} \cdot \mathbf{h} + \mathbf{c}^D : \mathbf{b}$ , the Helfrich fourth-order stiffness tensor is

$$\mathbf{c}^D = \frac{\partial \mathbf{M}^{\text{fe}}}{\partial \mathbf{b}} = \left( k_c^D + \frac{\bar{k}_c^D}{2} \right) \mathbf{I}_s \mathbf{I}_s - \frac{\bar{k}_c^D}{2} \mathbf{q}^* \mathbf{q}^*, \quad (20)$$

which consists of bending and torsion contributions. Using this result the tension  $\gamma$  [Eq. (18)] can be expressed in terms of curvature and displacement:

$$\gamma = \gamma_{00} + \frac{1}{2} \mathbf{b} : \mathbf{c}^D : \mathbf{b} - \frac{1}{2} \beta^b D D. \quad (21)$$

### 3. Flexoelastic stress tensor

Using a variational calculation of the free energy with respect to density  $\rho$  and curvature  $\mathbf{b}$ , the 2D flexoelastic stress tensor  $\mathbf{T}$  is found to be [15,18]

$$\mathbf{T} = \left( \bar{A} - \rho \frac{\partial \bar{A}}{\partial \rho} \right) \mathbf{I}_s - \mathbf{M}^{\text{fe}} \cdot \mathbf{b}, \quad (22)$$

where the first term is the 2D normal stress arising from changes in  $\rho$ , and the second term represents the 2D normal and shear stresses arising from in-plane deformations. Replacing Eqs. (16) and (19) into Eq. (22), we separate the extension and shear stresses:

$$\mathbf{T} = \left( \gamma_{00} - h_f \mathbb{H} D + \frac{1}{2} \beta^b D D \right) \mathbf{I}_s - \left( \frac{\mathcal{T} \mathbb{D}}{2} \right) \mathbf{q}^*. \quad (23)$$

Hence the linearized Laplace pressure generated by the stress is  $\mathbf{T} : \mathbf{b} = 2\gamma_{00} \mathbb{H}$ , as indicated in Eq. (9b).

### 4. Flexoelectric coupling constant

Using Eqs. (9) and (19), the linear integral shape equation for spherical membranes under a pressure drop  $\mathbf{k} \mathbf{k}$ :  $(\mathbf{T}_{b(2)} - \mathbf{T}_{b(1)}) = \Delta p$  from the contacting fluids is

$$\Delta p(t) = 2\gamma_{00} \mathbb{H} + [-h_f D + (2k_c^D + \bar{k}_c^D) \mathbb{H}] \mathbb{S}_{\text{sphere}}. \quad (24)$$

Under short circuit conditions (see Fig. 5,  $E = 0$ ), Eq. (8b) gives  $D = (2h_f / \beta^b) \mathbb{H}$ , and replacing this into Eq. (24) gives

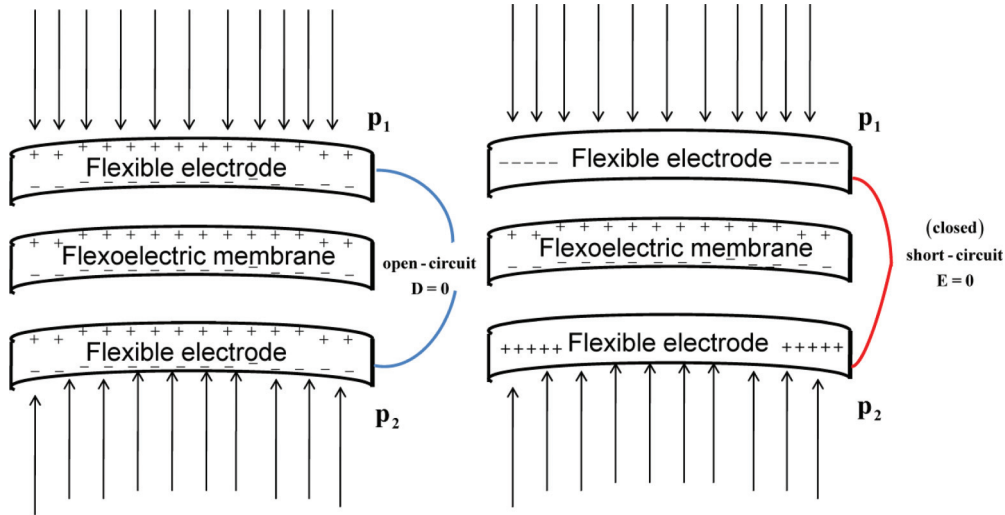


FIG. 5. (Color online) Schematic diagram showing the open and closed circuit states for a flexoelectric membrane under bending between two flexible electrodes; the bending is created by an externally imposed pressure drop  $p_1 - p_2$  from the contacting fluid phases. The left-hand side shows the open circuit when the surface displacement is zero, whereas the right-hand side shows the closed circuit when the electric field is zero. The charge separation in the membrane is due to the flexoelectric effect.

the elastic energy  $W_{\text{elas}}$  (energy/area):

$$W_{\text{elas}} = \frac{\Delta p \mathbb{H}}{S_{\text{sphere}}} = \left\{ (2\gamma_{00} + (2k_c^D + \bar{k}_c^D) S_{\text{sphere}}) - \frac{2S_{\text{sphere}} h_f^2}{\beta^b} \right\} \frac{\mathbb{H}^2}{S_{\text{sphere}}}. \quad (25)$$

According to Eq. (16) the electric energy (energy per area) is a quadratic function of curvature:

$$W_{\text{elec}} = \frac{\beta^b D^2}{2} = \frac{2(h_f)^2}{\beta^b} \mathbb{H}^2. \quad (26)$$

The flexoelectric conversion constant  $k^2$  that describes the conversion of mechanical into electric energy is then

$$k^2 = \frac{W_{\text{elec}}}{W_{\text{elas}} + W_{\text{elec}}} = \frac{h_f^2}{\beta^b \left( \frac{\gamma_{00}}{S_{\text{sphere}}} + k_c^D + \frac{\bar{k}_c^D}{2} \right)} < 1. \quad (27)$$

Estimations of  $k^2$  by Petrov for biological membranes in the absence of tension and torsion give values close to 1 ([10], p. 487). We note that to increase conversion one can decrease the stiffness and/or increase the flexoelectric coupling constant through chemistry. Rewriting the total free energy using the surface Euler equation and Eq. (16) gives

$$A = \bar{A}/S_{\text{sphere}} = \frac{1}{S_{\text{sphere}}} \left( \rho \frac{\partial \bar{A}_{00}}{\partial \rho} + \bar{A}_{00}(\rho) \right) + \left\{ \frac{2\gamma_{00}}{S_{\text{sphere}}} + \left( k_c^D + \frac{\bar{k}_c^D}{2} \right) \left( \frac{\mathbb{H}^2}{S_{\text{sphere}}} \right) \right\} - 2h_f \mathbb{H} D. \quad (28)$$

We see that the conversion coefficient  $k^2$  given in Eq. (27) is consistent with the standard formula (2) obtained from

the free energy (28). A similar calculation can be done for cylinders.

### III. FLEXOELECTRIC ENERGY HARVESTER

#### A. Flexoelectric dynamic shape equation

Using the generic linear integral shape time-dependent equation (9a) [14], [19] we find

$$-\rho \frac{\partial v}{\partial t} \mathbb{H} + 2\gamma_{00} \mathbb{H} + \left[ \left( \frac{\mathcal{B}}{2} - h_f D \right) + \boldsymbol{\eta} \cdot \mathbf{M}^v \cdot \boldsymbol{\eta} \right] \mathbb{S} = \Delta p(t), \quad (29)$$

where  $\Delta p(t)$  is the time-dependent pressure drop; a more complicated mechanical energy transfer that includes viscosity or viscoelasticity in the linear and nonlinear regimes can be incorporated in the future [21,25–30]. The viscous moment tensor  $\mathbf{M}^v$  can be obtained from the viscous dissipation function due to the time rate of curvature  $d\mathbf{b}/dt$ . In the linear regime the viscous moment tensor for bending and torsion modes is [19]

$$\mathbf{M}^v = \lambda^{\mathcal{B}} \frac{d\mathbb{H}}{dt} \mathbf{I}_s + \lambda^{\mathcal{T}} \frac{d\mathbb{D}}{dt} \mathbf{q}^*, \quad (30)$$

where  $\lambda^{\mathcal{B}}$  and  $\lambda^{\mathcal{T}}$  (energy  $\times$  time) are the viscosities for bending and torsion. Using previous work on Newtonian sheets of thickness  $t$ , we find that the bending viscosity is [31]

$$\lambda^{\mathcal{B}} = \frac{\mu H^3}{3}, \quad (31)$$

where  $\mu$  is a characteristic shear viscosity. Again, for a spherical rate of deformations  $d\mathbb{H}/dt = d\mathbb{D}/dt$  and for a cylindrical rate of deformations  $d\mathbb{H}/dt = d\mathbb{D}/dt$ . Next we focus on the spherical ( $d\mathbb{D}/dt = 0$ ) case since polarization couples

with bending and not torsion and hence this case leads to higher efficiency, but the analysis can be trivially extended to the cylindrical case. As before, we consider a circular membrane attached and fixed on the inner sides of a capillary of radius  $a$ . Bulk fluids are placed on top of and below the membrane located at  $z = 0$ . As before, we only consider only the mechanical effect from the fluids on the membrane to be the time-dependent pressure drop  $\Delta p(t) = 0$ . The normal velocity  $V$  of the membrane is found by introducing the associated flow rate  $Q(t)$  given by  $Q(t) = V(t)\pi a^2/2$ . As the membrane oscillates due to oscillations in  $\Delta p(t)$ , the membrane deformation corresponds to a spherical cap. Under the small deformation condition the ratio of the height  $h$  of the cap to the capillary radius  $a$  is small:  $h/a \ll 1$ . The time-dependent volume of the spherical cap is  $\Omega(t) = \pi a^2 h(t)/2$ . To find the associated flow rate  $Q(t)$  in terms of the curvature dynamics, we first consider the flow rate in terms of the time derivative of the volume,  $2d\Omega(t)/dt = Q(t)$ , which upon use of Eq. (19c) gives the relation between  $dh/dt$  and the normal velocity  $V$ ,

$$\frac{dh(t)}{dt} = \frac{V(t)}{2}. \quad (32)$$

Using the geometric relation for the spherical cusp  $a^2 = -2h/\mathbb{H}$  and Eq. (32) the normal velocity  $V$  can be expressed in terms of  $d/\mathbb{H}dt$ :

$$\frac{d\mathbb{H}(t)}{dt} a^2 = -V(t). \quad (33)$$

Replacing Eq. (33) into Eq. (29) and considering Eq. (8b) we obtain for the flexoelectric harvester

$$\begin{aligned} (\rho a^2) \frac{d^2 \mathbb{H}}{dt^2} + (\lambda^B S) \frac{d\mathbb{H}}{dt} + [2\gamma_{00} + (2k_c^D + \bar{k}_c^D) S_{\text{sphere}}] \mathbb{H} \\ - (h_f S) D = \Delta p(t), \\ E = \beta^b D - 2h_f \mathbb{H}. \end{aligned} \quad (34)$$

Expressing the field as  $E = v/t$  ( $v$ : voltage) and the displacement as  $D = v/Ct$  ( $C$ : capacitance) and putting into Eqs. (34) for a given  $\Delta p(t)$ , the curvature  $\mathbb{H}(t)$  and voltage  $v(t)$  as a function of time can be obtained. The resonant frequency  $\omega_{r,oc}$  under open circuit conditions ( $D = 0$ ) is given by the ratio of membrane elasticity to inertia:

$$\omega_{r,oc} = \sqrt{[2\gamma_{00} + (2k_c^D + \bar{k}_c^D) S_{\text{sphere}}] / \rho a^2}, \quad (35)$$

which can be tuned through the tension and bending properties to maximize power absorption. We note that tension, bending, and torsion elasticity are involved.

### B. Open and closed circuit conditions

To calculate the electric power  $\Pi_{\text{elec}}$  produced, we use the standard formula  $\Pi_{\text{elec}} = \eta_f I_{\text{sc}} v_{\text{oc}}$ , where  $\eta_f$  is the filling factor,  $I_{\text{sc}}$  the short circuit current, and  $v_{\text{oc}}$  the open circuit voltage. Figure 5 shows a schematic of both conditions; in the open circuit the electrodes are disconnected and  $D = 0$ , and in the short circuit the connected electrode results in  $E = 0$ .

### 1. Open circuit

For periodic forcing due to fluid forces  $\Delta p(t) = \Delta p_0 \cos \omega t$ , under open circuit (oc) conditions ( $D=0$ ) the harvester equation (34) become a driven second order oscillator:

$$\begin{aligned} \rho a^2 \frac{d^2 \mathbb{H}}{dt^2} + (\lambda^B S_{\text{sphere}}) \frac{d\mathbb{H}}{dt} + [2\gamma_{00} + (2k_c^D + \bar{k}_c^D) S_{\text{sphere}}] \mathbb{H} \\ = \Delta p_0 \cos \omega t, \quad E = -2h_f \mathbb{H}. \end{aligned} \quad (36)$$

The frequency response of the curvature  $\mathbb{H}$  is characterized by the amplitude  $A$  and phase angle  $\phi$ :

$$\mathbb{H}(t) = A \cos(\omega t + \phi), \quad (37a)$$

$$A = \frac{\Delta p_0}{\rho a^2} \left\{ (\omega_{r,oc}^2 - \omega^2)^2 + (\lambda^B S_{\text{sphere}} / \rho a^2)^2 \omega^2 \right\}^{-1/2}, \quad (37b)$$

$$\tan \phi = -\frac{(\lambda^B S_{\text{sphere}} / \rho a^2) \omega}{\omega_{r,oc}^2 - \omega^2}. \quad (37c)$$

The curvature peaks at resonance and the phase lag increases with bending dissipation. The electric field  $E$  is found by replacing this result into  $E = -2h_f \mathbb{H}$ . The open circuit mechanical power  $\Pi_{\text{mech,oc}}$  (energy/time) for this second-order curvature oscillator is

$$\begin{aligned} \Pi_{\text{mech,oc}}(\omega) \\ = \frac{(\lambda^B S_{\text{sphere}})}{(S_{\text{sphere}})^2} \left\langle \left( \frac{d\mathbb{H}_{\text{oc}}}{dt} \right)^2 \right\rangle \\ = \frac{\Delta p_0^2}{2\lambda^B (S_{\text{sphere}})^3} \frac{(\lambda^B S_{\text{sphere}} / \rho a^2)^2 \omega^2}{(\omega_{r,oc}^2 - \omega^2)^2 + (\lambda^B S_{\text{sphere}} / \rho a^2)^2 \omega^2}, \end{aligned} \quad (38)$$

$$\omega_{r,oc}^2 = [2\gamma_{00} + (2k_c^D + \bar{k}_c^D) S_{\text{sphere}}] / \rho a^2, \quad (39)$$

where we used Eqs. (37) for  $\mathbb{H}_{\text{oc}}$ . Again the dissipated mechanical power is typical of this second-order oscillator. At resonance  $\omega = \omega_{r,oc}$  we find the usual scaling with the square of the forcing amplitude and with the reciprocal of the bending viscosity and a large geometric dependence:

$$\Pi_{\text{mech,oc}}(\omega = \omega_{r,oc}) = \frac{\Delta p_0^2}{2\lambda^B (S_{\text{sphere}})^3} = \frac{3}{2^{10}} \frac{\Delta p_0^2 a^6}{\mu H^3}. \quad (40)$$

The root mean open circuit voltage  $v_{\text{oc}} = \langle EH \rangle = \langle -2Hh_f \mathbb{H} \rangle$  is

$$\begin{aligned} v_{\text{oc}}(\omega) = \sqrt{2} h_f H \frac{\Delta p_0}{\rho a^2} \left\{ (\omega_{r,oc}^2 - \omega^2)^2 \right. \\ \left. + (\lambda^B S_{\text{sphere}} / \rho a^2)^2 \omega^2 \right\}^{-1/2}. \end{aligned} \quad (41)$$

At resonance the voltage decreases with increasing bending viscosity  $\lambda^B$  and frequency  $\omega_{r,oc}$ :

$$v_{oc}(\omega_{r,oc}) = \sqrt{2}h_f H \frac{\Delta p_0 a^2}{8\lambda^B \omega_{r,oc}}. \quad (42)$$

This equation also elucidates the role of flexoelectric coupling and membrane geometry.

## 2. Short circuit

Under short circuit conditions ( $E = 0$ ), replacing  $\beta^b D = 2h_f \mathbb{H}$  into Eqs. (34) give

$$\rho a^2 \frac{d^2 \mathbb{H}}{dt^2} + (\lambda^B S_{\text{sphere}}) \frac{d \mathbb{H}}{dt} + \left( [2\gamma_{00} + (2k_c^D + \bar{k}_c^D) S_{\text{sphere}}] - 2 \frac{(h_f^2 S_{\text{sphere}})}{\beta^b} \right) \mathbb{H} = \Delta p_0 \cos \omega t. \quad (43)$$

Using the same procedure as above for the oc, the mechanical power  $\Pi_{\text{mech,sc}}$  is

$$\Pi_{\text{mech,sc}}(\omega) = \frac{(\lambda^B S_{\text{sphere}})}{(S_{\text{sphere}})^2} \left\langle \left( \frac{d \mathbb{H}_{\text{sc}}}{dt} \right)^2 \right\rangle = \frac{\Delta p_0^2}{2\lambda^B (S_{\text{sphere}})^3} \frac{(\lambda^B S_{\text{sphere}} / \rho a^2)^2 \omega^2}{(\omega_{r,sc}^2 - \omega^2)^2 + (\lambda^B S_{\text{sphere}} / \rho a^2)^2 \omega^2}, \quad (44)$$

$$\omega_{r,sc}^2 = \left( 2\gamma_{00} + (2k_c^D + \bar{k}_c^D) S_{\text{sphere}} - 2 \frac{(h_f^2 S_{\text{sphere}})}{\beta^b} \right) / \rho a^2. \quad (45)$$

Since the stiffness is reduced under the short circuit, the resonance frequency is smaller than for the open circuit. On the other hand, at resonance the power remains equal for both cases.

The root mean short circuit current  $I_{sc}$  is found from

$$I_{sc} = \left\langle \frac{d}{dt} D \mathbb{H} \right\rangle = \left\langle \frac{2H h_f}{\beta^b} \frac{d \mathbb{H}}{dt} \right\rangle = \frac{\sqrt{2} H h_f}{\beta^b} \left\{ \frac{\Delta p_0 \omega}{\rho a^2} \left\{ (\omega_{r,sc}^2 - \omega^2)^2 + (\lambda^B S_{\text{sphere}} / \rho a^2)^2 \omega^2 \right\}^{-1/2} \right\}. \quad (46)$$

At resonance, the short circuit current  $I_{sc}(\omega_{r,sc})$  decreases with bending viscosity  $\lambda^B$  and is proportional to the resonant open circuit voltage  $v_{oc}(\omega_{r,oc})$ :

$$I_{sc}(\omega_{r,sc}) = \frac{\sqrt{2} H h_f}{\beta^b} \frac{\Delta p_0 a^2}{8\lambda^B} = \frac{\omega_{r,oc} v_{oc}(\omega_{r,oc})}{\beta^b}. \quad (47)$$

This equation also elucidates the role of flexoelectric coupling, inverse permittivity, and membrane geometry.

## 3. Electrical power $\Pi_{\text{elec}}$

We define the electric power  $\Pi_{\text{elec}}$  of the device using the standard formula involving the product of the open circuit voltage  $v_{oc}$  and short circuit current  $I_{sc}$ :

$$\begin{aligned} \Pi_{\text{elec}}(\omega) &= \eta_f I_{sc} v_{oc} = \eta_f \underbrace{\left( \frac{H \Delta P_0}{\rho a^2} \right)^2}_{\text{fluid power}} \underbrace{k^2 \left( \frac{\gamma_{00}}{S_{\text{sphere}}} + (k_c^D + \bar{k}_c^D / 2) \right)}_{\text{flexoelectric transduction}} \\ &\quad \times \underbrace{\left( \frac{\omega}{\left\{ (\omega_{r,oc}^2 - \omega^2)^2 + (\lambda^B S_{\text{sphere}} / \rho a^2)^2 \omega^2 \right\}^{1/2} \left\{ (\omega_{r,sc}^2 - \omega^2)^2 + (\lambda^B S_{\text{sphere}} / \rho a^2)^2 \omega^2 \right\}^{1/2}} \right)}_{\text{frequency response function}}. \end{aligned} \quad (48)$$

The power expression (48) is decomposed into the three labeled key factors:

- (i) the fluid mechanical input  $(H \Delta P_0 / \rho a^2)^2$ ;
- (ii) the membrane electromechanical transduction properties; since the transduction term is  $k^2 [\gamma_{00} / S_{\text{sphere}} + (k_c^D + \bar{k}_c^D) / 2]$  we see that the power is proportional to the coupling factor  $k^2$  [Eq. (27)], and that it is just  $h_f^2 / \beta^b$ ;
- (iii) the frequency response function; the power has two resonant peaks that reflect the effect of flexoelectricity on the bending stiffness and a second-order oscillator.

## 4. Power conversion efficiency

An estimate of the mechanical-to-electrical power conversion efficiency  $\Sigma$  can be defined using the geometric average of the open and short circuit powers  $\sqrt{\Pi_{\text{mech,oc}} \Pi_{\text{mech,sc}}}$ :

$$\Sigma = \frac{\Pi_{\text{elec}}}{\sqrt{\Pi_{\text{mech,oc}} \Pi_{\text{mech,sc}} + \Pi_{\text{elec}}}}. \quad (49)$$

Using Eqs. (38), (39), (44), (45), (48), and (49) we find that the efficiency  $\Sigma$  is given by the time scale ratio



function:

$$\Sigma = \frac{\tau_v/\tau_{fe}}{1 + \tau_v/\tau_{fe}}, \quad \tau_v = \frac{1}{\omega},$$

$$\tau_{fe} = \frac{\lambda^B}{2\eta_f H^2 \omega_{r,oc}^2 \rho a^2 k^2} = \frac{\lambda^B \beta^b}{2\eta_f H^2 S_{\text{sphere}} h_f^2}, \quad (50)$$

where  $\tau_v$  is the bulk fluid time scale and  $\tau_{fe}$  the flexoelectric time scale. Notice that in Eqs. (50) was used the relationship  $k^2 \omega_{r,oc}^2 \rho a^2 = 2S_{\text{sphere}}(h_f^2/\beta^b)$  through Eqs. (27) and (35) respectively. The efficiency  $\Sigma$  displays a typical algebraic decay with increasing time scale ratio  $\tau_v/\tau_{fe}$ . The two asymptotic limits of  $\Sigma$  are

$$\lim_{\tau_v/\tau_{fe} \rightarrow \infty} \Sigma = \lim_{\tau_v/\tau_{fe} \rightarrow \infty} \frac{\tau_v/\tau_{fe}}{1 + \tau_v/\tau_{fe}} = 1, \quad \lim_{\tau_v/\tau_{fe} \rightarrow 0} \Sigma = 0, \quad (51)$$

indicating that at very large forcing frequency there is insufficient time to effect mechano-electrical conversion. The role of the static conversion factor  $k^2$  in the power conversion efficiency is found from Eqs. (50) and as expected increases with decreasing frequency:

$$\Sigma = \frac{k^2}{\left(\frac{\lambda^B}{2\eta_f H^2 \omega_{r,oc}^2 \rho a^2}\right)\omega + k^2}. \quad (52)$$

The crossover frequency  $\omega^*$  at which both times are equal,  $\tau_v = \tau_{em}$ , and the efficiency achieves 50% is proportional to the conversion factor  $k^2$ :

$$\omega^* = \left[ \frac{2\eta_f H^2 \omega_{r,oc}^2 \rho a^2}{\lambda^B} \right] k^2. \quad (53)$$

This efficiency threshold is theoretically achieved by calibrating the resonance frequency, flexoelectric coupling, and bending viscosity. We can further define an index of merit of the device based on the material properties by evaluating the efficiency at the resonant open circuit frequency  $\omega_{r,oc}$ :

$$\Sigma|_{\omega_{r,oc}} = \frac{\Pi_{\text{elec}}}{\sqrt{\Pi_{\text{mech,oc}} \Pi_{\text{mech,sc}} + \Pi_{\text{elec}}}} \Big|_{\omega_{r,oc}}. \quad (54)$$

The frequency-dependent membrane Reynolds number is the ratio of inertial to viscous effects:

$$\text{Re} = \frac{\rho(\omega a) a H^2}{\lambda^B}. \quad (55)$$

This, when introduced into the index of merit using Eq. (55), gives a relation between the power conversion efficiency and the energy conversion efficiency:

$$\Sigma|_{\omega_{r,oc}} = \frac{\eta_f \text{Re}_{r,oc} k^2}{1 + \eta_f \text{Re}_{r,oc} k^2}. \quad (56)$$

For large viscosity and small Reynolds number (creeping mode), the small index of merit increases with  $\text{Re}_{r,oc} k^2$ :  $\Sigma|_{\omega_{r,oc}} = \eta_f \text{Re}_{r,oc} k^2 - \eta_f^2 (\text{Re}_{r,oc})^2 k^4 + \dots$ . In the inviscid large-Reynolds-number mode, the larger index of merit decreases with  $\text{Re}_{r,oc} k^2$ :

$$\Sigma|_{\omega_{r,oc}} = 1 - 1/\eta_f \text{Re}_{r,oc} k^2 + \dots \quad (57)$$

#### IV. CONCLUSIONS

A soft-matter-based energy mechanical energy harvesting system is formulated using flexoelectric membranes as the electromechanical transduction mechanism. The proposed energy generator consists in the absorption of mechanical energy from contacting fluids by the membrane whose deformation generates a voltage through flexoelectricity. The key modeling building blocks of fluid mechanical energy harvesting based on electroelastic deformable solids are the formulation of thermodynamic coupling coefficients (conversion of mechanical into electric energy), the integration of the solid-fluid interaction with the electromechanical conversion process, the electric power formula, and the efficiency and index of merit of the device. This paper proposes the use of flexoelectric deformable membranes as the basic unit of transduction, where bending creates electric polarization and electric fields create bending deformations. The device formulation objectives were accomplished by first formulating the equations of membrane flexoelasticity which were then used as input for a viscoelastic dynamical model for curvature dynamics. The device model is based on the formulation of the membrane Helmholtz free energy density in terms of Helfrich bending and torsion elasticity, and its coupling with the area electric induction. The flexoelectric conversion coefficient  $k^2$  that describes the fraction of the mechanical energy converted into electrical energy through flexoelectricity is formulated and found to follow the standard expression as the ratio of the coupling energy to the product of electric and elastic energies; here the roles of membrane tension, bending, and torsion are identified. The subsequent derivations of the tension, flexoelastic moment tensor, and stress tensor, based on the thermodynamics of polarizable membranes, are incorporated into a linear integral shape equation for spherical and cylindrical membranes to obtain the mechanical energy harvester model. The tension of a curved polarized membrane is shown to contain Helfrich and displacement contributions. The bending moment contains the flexoelectric term that supports the energy conversion. The energy harvester consists of the driven viscoelastoinertial second-order dynamics of the membrane curvature coupled through flexoelectricity to the electric field. A model geometry consisting of a circular membrane fixed in a capillary of radius  $a$  containing bulk fluid that produces a time-dependent pressure drop  $\Delta p(t)$  was investigated. The frequency response of the system under open and short circuit conditions was characterized, including the open circuit voltage, short circuit current, and mechanical power at resonance. The resonant frequency is the ratio of the total deformation resistance to the inertia, and since in an open circuit there is no electromechanical coupling, the resonance is shifted to a higher value than under a short circuit.

In both cases the mechanical resonant power is inversely proportional to the bending viscosity  $\lambda^B$  and the eighth power of the membrane radius. The electric power was defined as the product of the fill factor times the open circuit voltage times the short circuit current; the expression is cast as the product of the fluid pressure forces (input), the flexoelectric transduction proportional to  $k^2$  (conversion), and the frequency response function (dynamical system), which is the geometric mean of the short and open circuit responses, revealing the role of

the thermodynamic conversion factor in power production. Lastly the power efficiency was estimated using the open circuit resonant condition, showing that with large bending viscosities the lower efficiency increases with  $k^2$ , while under low viscosity, the larger efficiency decreases with  $k^2$ .

The flexoelectric energy harvester proposed and simulated in this paper has already been experimentally realized in two prototypes based on bilayer lipid membranes and oscillating fluid flows. These experimental prototypes are discussed in detail in Ref. [10], Chap. 7, and consist of a black lipid membrane suspended on a millimeter-size Teflon orifice and a membrane patch sealed inside a micrometer-size glass pipette; both of which have been shown to generate flexoelectric power in both the open and short circuit regimes, in a broad frequency range.

The specific predictions obtained can form the design basis for a soft-matter-based mechanical energy harvester using flexoelectricity. It has been shown that both the bending elasticity in the energy conversion and the bending viscosity play a significant role in electric power production and efficiency. These theoretical predictions support current efforts in developing flexoelectric energy harvesters. More quantitative predictions will require experimental data as well as atomistic or molecular dynamics simulations.

#### ACKNOWLEDGMENTS

A.D.R. was supported by the US Office of Basic Energy Sciences, Department of Energy, Grant No. DE-SC0001412. E.E.H.V. gratefully acknowledges financial fellowship support from CONACYT-MEXICO (Postdoctoral Grant No. 000000000147870) and the Canada Government through Foreign Affairs and International Trade Canada (DFAIT).

#### APPENDIX A

This Appendix summarizes the differential geometry used in this paper (following Kralchevsky and Nagayama [20], Edwards *et al.* [32], Stumpf and Badur [33], and Eliassen [34]). Consider a two-dimensional (2D) membrane whose points are located in 3D space by a position vector  $\mathbf{R}$ , given by

$$\mathbf{R} = \mathbf{R}(u^\alpha), \quad \alpha = 1, 2. \quad (\text{A1})$$

The two tangential base vectors  $\mathbf{a}_\alpha$  induced by the surface coordinates are defined by

$$\mathbf{a}_\alpha = \frac{\partial \mathbf{R}}{\partial u^\alpha}, \quad \alpha = 1, 2, \dots \quad (\text{A2})$$

The definition of the corresponding surface metric tensor  $a_{\alpha\beta}$  is

$$\mathbf{a}_{\alpha\beta} = \mathbf{a}_\alpha \cdot \mathbf{a}_\beta; \quad \alpha, \beta = 1, 2 \quad (\text{A3})$$

whose determinant is

$$\det(\mathbf{a}_{\alpha\beta}) > 0. \quad (\text{A4})$$

The corresponding reciprocal base vectors  $\mathbf{a}^\alpha$  and metric tensor are

$$\mathbf{a}^\alpha = \frac{\partial u^\alpha}{\partial \mathbf{R}}, \quad (\text{A5a})$$

$$\mathbf{a}^{\alpha\beta} = \mathbf{a}^\alpha \cdot \mathbf{a}^\beta, \quad \alpha, \beta = 1, 2 \quad (\text{A5b})$$

The base and reciprocal base vectors define the surface unit tensor  $\delta_\alpha^\beta$ , and the dyadic surface idem factor  $\mathbf{I}_s$ :

$$\mathbf{a}_\alpha \cdot \mathbf{a}^\beta = \delta_\alpha^\beta, \quad (\text{A6a})$$

$$\mathbf{I}_s = \mathbf{a}_\beta \mathbf{a}^\alpha \delta_\alpha^\beta = \mathbf{a}_\alpha \mathbf{a}^\beta \delta_\beta^\alpha = a_{\alpha\beta} \mathbf{a}_\alpha \mathbf{a}^\beta = a^{\alpha\beta} \mathbf{a}_\alpha \mathbf{a}_\beta, \quad (\text{A6b})$$

where  $a^{\alpha\beta} a_\gamma = \delta_\gamma^\alpha$ . The counterclockwise rotation of a vector around the unit normal  $\mathbf{k}$  is given by the dyadic surface unit alternator  $\boldsymbol{\varepsilon}_s$ :

$$\begin{aligned} \boldsymbol{\varepsilon}_s &= -\mathbf{k} \times \mathbf{I}_s = -\mathbf{I}_s \times \mathbf{k} = -\mathbf{k} \times \mathbf{I} \\ &= -\mathbf{I} \times \mathbf{k} = \mathbf{a}^\alpha \mathbf{a}^\beta \varepsilon_{\alpha\beta} = \mathbf{a}_\alpha \mathbf{a}_\beta \varepsilon^{\alpha\beta}, \end{aligned} \quad (\text{A7})$$

where  $\varepsilon_{\gamma\delta} = a_{\alpha\gamma} a_{\beta\delta} \varepsilon^{\alpha\beta}$ . The surface unit normal  $\mathbf{k}$  is given by

$$\begin{aligned} \mathbf{k} &= \frac{1}{2} \boldsymbol{\varepsilon}_s : \boldsymbol{\varepsilon} = \frac{1}{2} \boldsymbol{\varepsilon}^{\alpha\beta} \mathbf{a}_\alpha \times \mathbf{a}_\beta \\ &= \frac{1}{2} \frac{1}{\sqrt{a}} (\mathbf{a}_1 \times \mathbf{a}_2 - \mathbf{a}_2 \times \mathbf{a}_1), \end{aligned} \quad (\text{A8})$$

where  $\boldsymbol{\varepsilon}$  is the triadic spatial unit alternator. Other useful relations involving the surface unit normal  $\mathbf{k}$  are

$$\mathbf{a}_\alpha \times \mathbf{a}_\beta = \mathbf{k} \varepsilon_{\alpha\beta}, \quad (\text{A9a})$$

$$\mathbf{a}_\alpha \times \mathbf{k} = -\mathbf{k} \times \mathbf{a}_\alpha = \mathbf{a}^\beta \varepsilon_{\beta\alpha}, \quad (\text{A9b})$$

$$\mathbf{I}_s \times \mathbf{I}_s = \mathbf{a}_\alpha \mathbf{k} \mathbf{a}_\beta \varepsilon^{\alpha\beta} = -\boldsymbol{\varepsilon} + \boldsymbol{\varepsilon}_s \mathbf{k} + \mathbf{k} \boldsymbol{\varepsilon}_s. \quad (\text{A9c})$$

The symmetric curvature dyadic  $\mathbf{b}$  is a measure of the change of  $\mathbf{k}$  with changes of  $\mathbf{R}$ :

$$\mathbf{b} = -\frac{\partial \mathbf{k}}{\partial \mathbf{R}} = -\nabla_s \mathbf{k}, \quad (\text{A10a})$$

$$\nabla_s(\dots) = \mathbf{I}_s \cdot \nabla(\dots) = \frac{\partial(\dots)}{\partial \mathbf{R}} = \mathbf{a}_\alpha \frac{\partial(\dots)}{\partial u^\alpha}, \quad (\text{A10b})$$

where  $\nabla_s(\dots)$  is the surface gradient. The components of  $\mathbf{b}$  obey

$$b^{\gamma\delta} = a^{\delta\beta} b_\beta^\gamma, \quad (\text{A11a})$$

$$b_\beta^\gamma = a^{\gamma\alpha} b_{\alpha\beta}. \quad (\text{A11b})$$

The spectral representation of  $\mathbf{b}$  in the principal frame defined by the main curvature is

$$\mathbf{b} = \nu_1 \mathbf{e}_1 \mathbf{e}_1 + \nu_2 \mathbf{e}_2 \mathbf{e}_2, \quad (\text{A12})$$

where the eigenvectors of  $\mathbf{b}$  are  $(\mathbf{e}_1, \mathbf{e}_2)$  and the eigenvalues  $c_1$  and  $c_2$  give the radius of curvature. The surface idem factor  $\mathbf{I}_s = \mathbf{e}_1 \mathbf{e}_1 + \mathbf{e}_2 \mathbf{e}_2$ . The two invariants of  $\mathbf{b}$  are the trace and the determinant:

$$\text{tr} \mathbf{b} = \nu_1 + \nu_2, \quad \det \mathbf{b} = \nu_1 \nu_2. \quad (\text{A13})$$

The Cayley-Hamilton theorem gives

$$\mathbf{b} \cdot \mathbf{b} - (\text{tr} \mathbf{b}) \mathbf{b} + (\det \mathbf{b}) \mathbf{I}_s = \mathbf{0}. \quad (\text{A14})$$

The invariants of  $\mathbf{b}$  are used to define the average curvature  $H$  and the Gaussian or total curvature  $K$ :

$$2H = \mathbf{I}_s : \mathbf{b} = -\nabla_s \cdot \mathbf{k} = -\mathbf{a}^\alpha \cdot \frac{\partial \mathbf{k}}{\partial u^\alpha} = b_\alpha^\alpha = (c_1 + c_2), \quad (\text{A15})$$

$$K = -\frac{1}{2} \boldsymbol{\varepsilon}_s : (\mathbf{b} \cdot \boldsymbol{\varepsilon}_s \cdot \mathbf{b}) = \frac{1}{2} \boldsymbol{\varepsilon}^{\alpha\beta} \boldsymbol{\varepsilon}^{\gamma\delta} b_{\alpha\gamma} b_{\beta\delta} = c_1 c_2. \quad (\text{A16})$$

The relation between  $K$  and  $\mathbb{H}$  obtained from the trace of Eq. (A14) is

$$K = 2H^2 - \frac{1}{2} \mathbf{b} : \mathbf{b}. \quad (\text{A17})$$

The curvature tensor  $\mathbf{b}$  can be decomposed into a trace ( $\mathbb{H}\mathbf{I}_s$ ) and a deviatoric curvature ( $\mathbb{D}\mathbf{q}$  [24]):

$$\mathbf{b} = \mathbb{H}\mathbf{I}_s + \mathbb{D}\mathbf{q}^*, \quad \mathbf{I}_s : \mathbf{I}_s = \mathbf{q}^* : \mathbf{q}^* = 2, \quad \mathbf{I}_s : \mathbf{q}^* = 0, \quad (\text{A18})$$

where the deviatoric curvature  $\mathbb{D}$  is

$$D = \frac{1}{2} (c_1 - c_2), \quad (\text{A19a})$$

$$D^2 = H^2 - K = \frac{1}{2} \mathbf{b} : \mathbf{b} - H^2. \quad (\text{A19b})$$

According to differential geometry, the four  $2 \times 2$  basis tensors are  $\{\mathbf{I}_s, \mathbf{q}^*, \boldsymbol{\varepsilon}_s, (\boldsymbol{\varepsilon}_s \cdot \mathbf{q}^*)\}$  and in the principal frame these tensors read [24]

$$\mathbf{I}_s = \begin{bmatrix} 1 & 0 \\ 0 & 1 \end{bmatrix}, \quad (\text{A20a})$$

$$\mathbf{q}^* = \begin{bmatrix} 1 & 0 \\ 0 & -1 \end{bmatrix}, \quad (\text{A20b})$$

$$\boldsymbol{\varepsilon}_s = \begin{bmatrix} 0 & 1 \\ -1 & 0 \end{bmatrix}, \quad (\text{A20c})$$

$$\boldsymbol{\varepsilon}_s \cdot \mathbf{q}^* = \begin{bmatrix} 0 & 1 \\ 1 & 0 \end{bmatrix}, \quad (\text{A20d})$$

and hence any  $2 \times 2$  tensor can be expanded as follows:

$$\begin{aligned} \mathbf{Z} = & \underbrace{\frac{1}{2} (\mathbf{Z} : \mathbf{I}_s) \mathbf{I}_s}_{\text{trace}} + \underbrace{\frac{1}{2} (\mathbf{Z} : \mathbf{q}^*) \mathbf{q}^*}_{\text{diagonal traceless}} \\ & + \underbrace{\frac{1}{2} (\mathbf{Z} : \boldsymbol{\varepsilon}_s) \boldsymbol{\varepsilon}_s}_{\text{antisymmetric}} + \underbrace{\frac{1}{2} [\mathbf{Z} : (\boldsymbol{\varepsilon}_s \cdot \mathbf{q}^*)] (\boldsymbol{\varepsilon}_s \cdot \mathbf{q}^*)}_{\text{symmetric off diagonal}}. \end{aligned} \quad (\text{A21})$$

Therefore a symmetric diagonal tensor reads

$$\mathbf{Z} = \frac{1}{2} (\mathbf{Z} : \mathbf{I}_s) \mathbf{I}_s + \frac{1}{2} (\mathbf{Z} : \mathbf{q}^*) \mathbf{q}^*. \quad (\text{A22})$$

## APPENDIX B

The purpose of this appendix is to derive Eq. (13). Rewriting Eqs. (11) and (12) in terms of densities (characters with overbars) using the area  $\mathbb{A}$ :

$$d(\mathbb{A}\bar{U}) = \Theta d(\mathbb{A}\bar{S}_{\text{ent}}) + (\gamma + \mathbf{E} \cdot \mathbf{D}) d\mathbb{A} + \mathbb{A} \mathbf{E} \cdot d\mathbf{D} + \mathbb{A} \mathbf{M} : d\mathbf{b}. \quad (\text{B1})$$

Performing the differentiation,

$$\bar{U} d\mathbb{A} + \mathbb{A} d\bar{U} = \bar{S}_{\text{ent}} \Theta d\mathbb{A} + \Theta \mathbb{A} d\bar{S}_{\text{ent}} + (\gamma + \mathbf{E} \cdot \mathbf{D}) d\mathbb{A} + \mathbb{A} \mathbf{E} \cdot d\mathbf{D} - \mathbb{A} \mathbf{M} : d\mathbf{b}. \quad (\text{B2})$$

Collecting terms:

$$d\bar{U} = \Theta d\bar{S}_{\text{ent}} + (\gamma - \bar{U} + \bar{S}_{\text{ent}} \Theta + \mathbf{E} \cdot \mathbf{D}) \frac{d\mathbb{A}}{\mathbb{A}} + \mathbf{E} \cdot d\mathbf{D} + \mathbf{M} : d\mathbf{b} \quad (\text{B3})$$

Introducing the mass balance,

$$\frac{d\mathbb{A}}{\mathbb{A}} = -\frac{d\rho}{\rho} \quad (\text{B4})$$

Eq. (B3) reads

$$d\bar{U} = \Theta d\bar{S}_{\text{ent}} + (-\gamma + \bar{U} - \bar{S}_{\text{ent}} \Theta - \mathbf{E} \cdot \mathbf{D}) \frac{d\rho}{\rho} + \mathbf{E} \cdot d\mathbf{D} + \mathbf{M} : d\mathbf{b}. \quad (\text{B5})$$

Introducing the Helmholtz free energy density  $\bar{A}$  we find

$$\bar{A} = \bar{U} - \Theta \bar{S}_{\text{ent}}, \quad (\text{B6})$$

$$d\bar{A} = d\bar{U} - \Theta d\bar{S}_{\text{ent}} - \bar{S}_{\text{ent}} d\Theta, \quad (\text{B7})$$

$$d\bar{U} = d\bar{A} + \Theta d\bar{S}_{\text{ent}} + \bar{S}_{\text{ent}} d\Theta. \quad (\text{B8})$$

Combining Eqs. (B5) and (B8), we have

$$d\bar{A} = -\bar{S}_{\text{ent}} d\Theta + (-\gamma + \bar{A} - \mathbf{E} \cdot \mathbf{D}) \frac{d\rho}{\rho} + \mathbf{E} \cdot d\mathbf{D} + \mathbf{M} : d\mathbf{b}. \quad (\text{B9})$$

Neglecting changes in  $\Theta$  we find Eq. (13):

$$d\bar{A} = (-\gamma + \bar{A} - \mathbf{E} \cdot \mathbf{D}) \frac{d\rho}{\rho} + \mathbf{E} \cdot d\mathbf{D} + \mathbf{M} : d\mathbf{b}. \quad (\text{B10})$$

[1] M. Farinholt, N. A. Pedrazas, D. M. Schluneker, D. W. Burt, and C. Farrar, *J. Intell. Mater. Syst. Struct.* **20**, 633 (2009).  
 [2] C. Jean-Mistral, S. Basrour, and J.-J. Chaillout, *Smart Mater. Struct.* **19**, 085012 (2010).  
 [3] A. Harb, *Renew. Energ.* **36**, 2641 (2011).  
 [4] H. D. Akaydin, N. Rlvln, and Y. Andreopolous, *J. Mater. Syst. Struct.* **21**, 1263 (2010).  
 [5] L. Gammaitoni, *Contemp. Phys.* **53**, 119 (2012).  
 [6] L. Giacomello and M. Porfiri, *J. Appl. Phys.* **109**, 084903 (2011).  
 [7] A. Erturk and D. J. Inman, *Piezoelectric Energy Harvesting* (John Wiley & Sons, Chichester, UK, 2011).

[8] D. J. Leo, *Engineering Analysis of Soft Material Systems* (Wiley, Hoboken, NJ, 2007).  
 [9] R. C. Smith, *Smart Material Systems* (SIAM, Philadelphia, PA, 2005).  
 [10] A. G. Petrov, *The Lyotropic State of Matter* (Gordon and Breach Science Publishers, Amsterdam, 1999).  
 [11] A. G. Petrov, *Biochim. Biophys. Acta* **85535**, 1 (2001).  
 [12] A. G. Petrov, in *Dynamics and Defects in Liquid Crystals*, edited by P. E. Cladis and P. Palfy-Murohay (Gordon and Breach, Amsterdam 1998), pp. 255–262.  
 [13] A. D. Rey, *Soft Matter* **6**, 3402 (2010).  
 [14] A. D. Rey, *Soft Matter* **3**, 1349 (2007).  
 [15] A. D. Rey, *Phys. Rev. E* **74**, 011710 (2006).

- [16] J. Harden, R. Teeling, J. T. Gleeson, S. Sprunt and A. Jákli, *Phys. Rev. E* **78**, 031702 (2008).
- [17] J. Harden, M. Chambers, R. Verduzco, P. Luchette, J. T. Gleeson, S. Sprunt, and A. Jákli, *Appl. Phys. Lett.* **96**, 102907 (2010).
- [18] A. D. Rey, *J. Colloid Interface Sci.* **304**, 226 (2006).
- [19] A. D. Rey, *Rheol. Acta* **47**, 861 (2008).
- [20] P. A. Kralchevsky and K. Nagayama, *Particles at Fluids Interfaces and Membranes* (Elsevier, Amsterdam, 2001).
- [21] M. Dakka, E. E. Herrera-Valencia, and A. D. Rey, *J. Non-Newtonian Fluid Mech.* **185-186**, 1 (2012).
- [22] D. Cuvelier, I. Derenyi, P. Bassereau, and P. Nassoy, *Biophys. J.* **88**, 2714 (2005).
- [23] V. A. Harmandaris and M. J. Deserno, *J. Chem. Phys.* **125**, 204905 (2006).
- [24] S. Ljunggren, J. C. Ericksson, and P. A. Kralchevsky, *J. Colloid Interface Sci.* **191**, 424 (1997).
- [25] A. D. Rey and E. E. Herrera-Valencia, *Biopolymers* **97**, 374 (2012).
- [26] A. D. Rey and E. E. Herrera-Valencia, in *Rheological Theory and Simulations of Surfactant Nematic Liquid Crystals in Self-Assembled Supramolecular Architecture: Lyotropic Liquid Crystals*, edited by N. Garti, P. Somasundaran, and R. Mezzenga (John Wiley & Sons, Hoboken, NJ, 2012), Chap. 2.
- [27] A. D. Rey, M. Golmohammadi, and E. E. Herrera-Valencia, *Soft Matter* **7**, 5002 (2011).
- [28] A. D. Rey and E. E. Herrera-Valencia, *Langmuir* **26**, 13033 (2010).
- [29] E. E. Herrera, F. Calderas, A. Chávez, and O. Manero, *J. Non-Newtonian Fluid Mech.* **165**, 174 (2010).
- [30] E. E. Herrera, F. Calderas, A. Chávez, O. Manero, and B. Mena, *Rheol. Acta* **48**, 779 (2009).
- [31] N. M. Ribe, *J. Fluid Mech.* **433**, 135 (2001).
- [32] D. A. Edwards, H. Brenner, and D. T. Wasan, *Interfacial Transport Processes and Rheology* (Butterworth, Boston, MA, 1991).
- [33] H. Stumpf and J. Badur, *Q. Appl. Math.* **51**, 161 (1993).
- [34] J. D. Eliassen, Ph.D. thesis, University of Minnesota, 1962.